



Giant enhancement of optical nonlinearity in two-dimensional materials by multiphoton-excitation resonance energy transfer from quantum dots

Hao Hong^{1,2,12}, Chunchun Wu^{1,2,12}, Zixun Zhao², Yonggang Zuo³, Jinhuan Wang⁴, Can Liu², Jin Zhang³, Fangfang Wang⁵, Jiangang Feng⁶, Huaibin Shen⁵, Jianbo Yin⁷, Yuchen Wu⁶, Yun Zhao⁴, Kehai Liu⁸, Peng Gao⁹, Sheng Meng³, Shiwei Wu¹⁰, Zhipei Sun¹¹, Kaihui Liu²✉ and Jie Xiong¹✉

Colloidal quantum dots are promising photoactive materials that enable plentiful photonic and optoelectronic applications ranging from lasers, displays and photodetectors to solar cells^{1–9}. However, these applications mainly utilize the linear optical properties of quantum dots, and their great potential in the broad nonlinear optical regime is still waiting for full exploration^{10–12}. Here, we demonstrate that a simple coating of a sub-200-nm-thick quantum dot film on two-dimensional materials can significantly enhance their nonlinear optical responses (second, third and fourth harmonic generation) by more than three orders of magnitude. Systematic experimental results indicate that this enhancement is driven by a non-trivial mechanism of multiphoton-excitation resonance energy transfer, where the quantum dots directly deliver their strongly absorbed multiphoton energy to the adjacent two-dimensional materials by a remote dipole-dipole coupling. Our findings could expand the applications of quantum dots in many exciting areas beyond linear optics, such as nonlinear optical signal processing, multiphoton imaging and ultracompact nonlinear optical elements.

Nonlinear optics is a fundamental building block of modern optics and lies at the core of many classical and quantum technologies. The introduction of nonlinear optics into two-dimensional (2D) materials provides a powerful tool for the study of novel physics in two dimensions^{13–16} and expands the versatility of nanophotonic applications, including nonlinear optical modulators, frequency combs and nanolasers^{17–19}. Owing to their enhanced electronic correlations and large transition dipole matrix elements, 2D materials express extremely strong optical nonlinearity at a normalized atomic thickness (for example, MoS₂ has typical second-order susceptibility $\chi^{(2)}$ of $\sim 10 \text{ nm V}^{-1}$ at $\sim 800 \text{ nm}$ excitation, which is three orders of magnitude larger than the β -barium

borate crystal)²⁰. However, their absolute light–matter interactions are actually too weak (for example, MoS₂ has a second harmonic conversion efficiency of only $\sim 10^{-7}$ at 10 GW cm^{-2} laser pump) to perform any practical application, and is mainly due to the reduced interaction length and lack of phase matching. Previously, much effort has been devoted to enhancing the optical nonlinearity of 2D materials through exploitation of the electric field, doping or strain, but improvements have typically been limited to an enhancement of only tenfold at most^{21–25}. Plasmonic nanocavities, waveguides and metamaterials hold promise for optical nonlinearity enhancement of several orders of magnitude^{26–29}, while the local hot spot of the electric field sacrifices the spatial homogeneity in a large area.

One plausible way to obtain homogeneous enhancement of optical responses in 2D systems is the massive transfer of energy from an adjacent photoactive medium^{30–32}. Having excellent optical properties such as ultrahigh absorption, near-unity photoluminescence (PL) quantum yield and nanosecond-scale long-lived photocarrier lifetimes, quantum dots (QDs) are considered to be promising photon-energy-storage materials and have been successfully used in the linear optical regime for light detection, harvesting and emitting. Whilst realizing giant enhancement of the nonlinear optical response in two dimensions by energy transfer, QDs have the potential advantage of serving as a photoactive medium. (1) QDs have a strong multiphoton nonlinear absorption but have silent frequency harmonic responses, which makes them ideal candidates for multiphoton energy storage¹¹. (2) Driven by long-range dipole–dipole electromagnetic interactions instead of interlayer electronic coupling only, in principle these stored energies in QDs can transfer remotely, rapidly and efficiently to the adjacent materials^{33–37}. (3) The selection rules for photoexcited-energy transfer are believed to be weakened in QDs due to the relaxed momentum matching at zero dimensions (0D)³⁸. Nevertheless, a giant nonlinear optical

¹State Key Laboratory of Electronic Thin Films and Integrated Devices, University of Electronic Science and Technology of China, Chengdu, China. ²State Key Lab for Mesoscopic Physics and Frontiers Science Center for Nano-optoelectronics, Collaborative Innovation Center of Quantum Matter, School of Physics, Peking University, Beijing, China. ³Institute of Physics, Chinese Academy of Sciences, Beijing, China. ⁴School of Chemistry and Chemical Engineering, Beijing Institute of Technology, Beijing, China. ⁵Key Laboratory for Special Functional Materials of Ministry of Education, Henan University, Kaifeng, China. ⁶Technical Institute of Physics and Chemistry, Chinese Academy of Sciences, Beijing, China. ⁷Beijing Graphene Institute (BGI), Beijing, China. ⁸Songshan Lake Materials Laboratory, Institute of Physics, Chinese Academy of Sciences, Dongguan, China. ⁹International Center for Quantum Materials, Research Center for Light-Element Advanced Materials, Peking University, Beijing, China. ¹⁰State Key Laboratory of Surface Physics and Department of Physics, Fudan University, Shanghai, China. ¹¹Department of Electronics and Nanoengineering and QTF Centre of Excellence, Aalto University, Aalto, Finland. ¹²These authors contributed equally: Hao Hong, Chunchun Wu. ✉e-mail: khliu@pku.edu.cn; jixiong@uestc.edu.cn

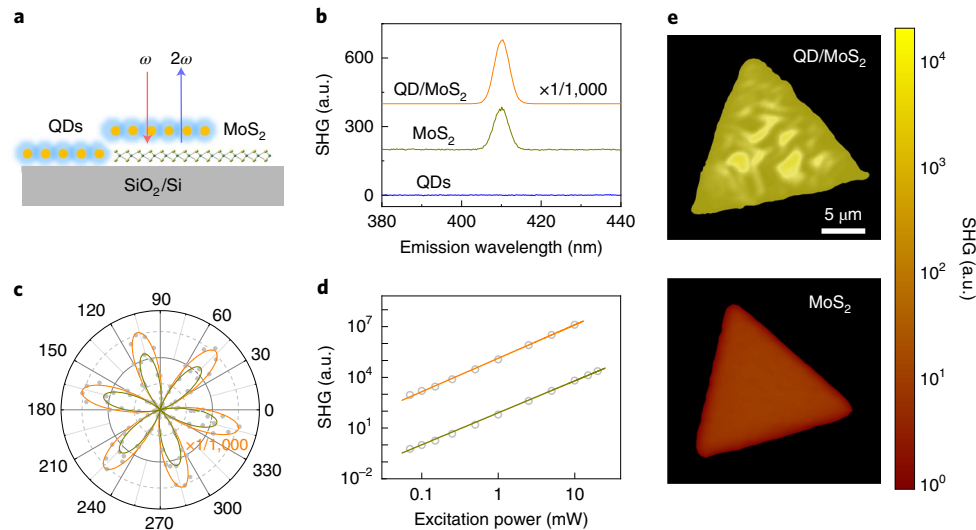


Fig. 1 | MoS₂ monolayer SHG enhancement with QD coating. **a**, Side-view illustration of the QD/MoS₂ hybrid structure and its optical SHG. **b**, SHG spectra of MoS₂ and QD/MoS₂ under 820 nm pulsed-laser excitation. With a QD coating, the weak SHG of MoS₂ can be boosted by ~1,500 times in the hybrid. For comparison, no apparent SHG signal can be observed for the pristine QDs. **c**, Polarization-dependent SHG patterns measured on a MoS₂ monolayer (dark yellow) and its QD hybrid (orange). **d**, Excitation power dependence of the SHG peak intensity for MoS₂ (dark yellow) and the QD/MoS₂ hybrid (orange), where both curves show the expected quadratic law. **e**, Spatial SHG intensity mapping images of a MoS₂ monolayer before (lower) and after (upper) QD coating.

response enhancement in two dimensions with the assistance of energy transfer from QDs has not yet been realized. Here, we demonstrate that a simple coating of sub-200-nm-thick QD films on 2D systems, that is, atomic-layered graphene, molybdenum disulfide (MoS₂), hexagonal boron nitride (hBN) and 4-dimethylamino-4'-nitrostilbene (DANS) molecular films, can significantly enhance their nonlinear optical responses (second, third and fourth harmonic generation) by up to three orders of magnitude, through a unique mechanism of multiphoton-excitation resonance energy transfer by a high-efficiency remote dipole–dipole coupling.

In our experiments, the hybrid QD/MoS₂ was fabricated by spin coating of CdSe/ZnS QDs on a MoS₂ monolayer (Fig. 1a; see Methods for fabrication details). Under excitation at frequency ω , the second-order susceptibility $\chi^{(2)}$ gives nonlinear polarization $P^{(2)} = \epsilon_0 \chi^{(2)} E^\omega E^\omega$, where ϵ_0 is the permittivity of free space and E^ω is the incident electric field. Here under 820 nm femtosecond pulse-laser excitation, the MoS₂ monolayer presents a sharp peak at 410 nm as expected for its second harmonic generation (SHG; Fig. 1b). This SHG intensity in MoS₂ is quite weak with a conversion efficiency of only $\sim 4 \times 10^{-7}$ (under a fundamental pump peak intensity of 20 GW cm^{-2}). However, after coating with a QD film (the thickness of $\sim 150 \text{ nm}$ is used for all the MoS₂ experiments unless otherwise specified), the SHG in the hybrid is dramatically enhanced to a conversion efficiency of up to $\sim 6 \times 10^{-4}$, with $\sim 1,500$ times enhancement compared with pristine MoS₂. Since pristine QD films have no observable SHG signal (Fig. 1b) under our experimental conditions, the strong SHG response in the hybrid can only be attributed to the enhanced SHG of MoS₂ with the adjacent QDs. This conclusion can also be directly drawn from the polarization-dependent SHG measurements, where characteristic six-fold anisotropic patterns with the same direction are observed in MoS₂ before and after coating with the QDs (Fig. 1c). As the SHG represents the conversion of two photons into one photon, a square dependence of the SHG intensity on the excitation power is observed in both MoS₂ and the QD/MoS₂ hybrid (Fig. 1d). In striking contrast with the enhancement at only local hot spots in plasmon- or cavity-related techniques, QDs can efficiently boost the SHG of the whole MoS₂ area (Fig. 1e).

The magnitude of the SHG enhancement can be tuned by the thickness of the QD film (Supplementary Fig. 1), where a thicker film leads to a larger enhancement, and a saturation trend is observed when the thickness reaches $\sim 100 \text{ nm}$. Interestingly, the SHG enhancement can also be tuned by the interaction distance between the QD and MoS₂. Here a SiO₂ spacer layer was inserted between the QD and MoS₂ by sequentially depositing a SiO₂ layer on the MoS₂ monolayer and then coating with the QD film (Fig. 2a). After the first step of SiO₂ deposition without the QD coating, the SHG intensity of MoS₂ was hardly changed (Supplementary Fig. 2). However, after coating with the QDs, the SHG was enhanced by ~ 170 times (Fig. 2b) even under interaction distance $R = 14 \text{ nm}$ (R contains the thickness of the SiO₂ layer and the radius of the ZnS/CdSe with an oleic acid ligand as shown in Fig. 2a). We further systematically monitored the SHG enhancement by tuning the SiO₂ thickness and observed that increasing the interaction distance quickly weakened the SHG enhancement with a fitted power coefficient of -2.3 (Fig. 2c). When R reaches $\sim 50 \text{ nm}$, hardly any of the strong SHG enhancement can be observed.

Previously, two prevailing scenarios had been proposed to understand the SHG enhancement in 2D materials, that is interfacial effects and local-field enhancement. Interfacial effects include charge transfer and symmetry breaking at the interface. Since our enhancement is feasible with the inserted SiO₂ layer, the interfacial effect can be first excluded. To verify whether the local-field effect is the origin of such a large SHG enhancement in MoS₂, we carefully calculated the SHG response by considering the optical field enhancement of both incident and emitted light (Supplementary Fig. 3). It turns out that the local-field effect only induces a fewfold SHG enhancement with the QD layer coating. We also monitored the two-photon absorption-induced photoluminescence (TPPL) of MoS₂ (its intensity is proportional to the fourth power of the local field, the same as for SHG) and observed only a several-times enhancement with the QD coating (Supplementary Fig. 4). We are thus confident to exclude the local-field enhancement as well. Therefore, there must be another mechanism that leads to the giant non-local SHG enhancement in MoS₂ by QD coating.

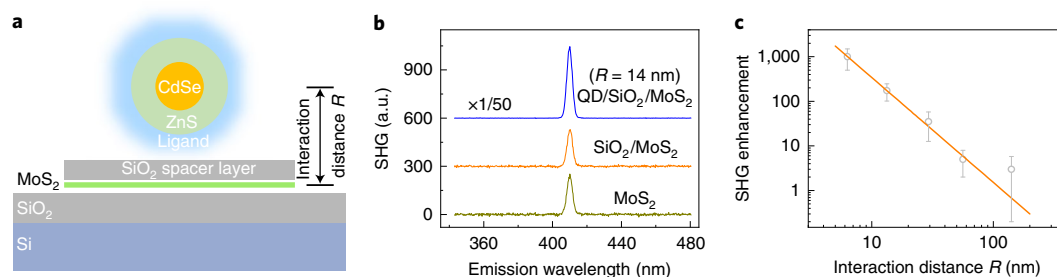


Fig. 2 | Interaction-distance-dependent SHG enhancement. **a**, Schematic illustration of the fabricated QD/SiO₂/MoS₂ sandwich hybrid structure by sequentially depositing SiO₂ and QDs on MoS₂. The interaction distance R between MoS₂ and the QD film can be systematically tuned by the thickness of the SiO₂ spacer layer. **b**, SHG spectra of MoS₂ and the fabricated hybrid structures. With an interaction distance of ~ 14 nm, the SHG intensity of MoS₂ can still be enhanced by ~ 170 times. For comparison, without QDs, the SiO₂ layer hardly influences the SHG intensity. **c**, Interaction-distance-dependent SHG enhancement. Increasing the interlayer distance quickly weakens the SHG enhancement, with a fitted power coefficient of -2.3 . Error bars are the standard deviation measured from ten samples.

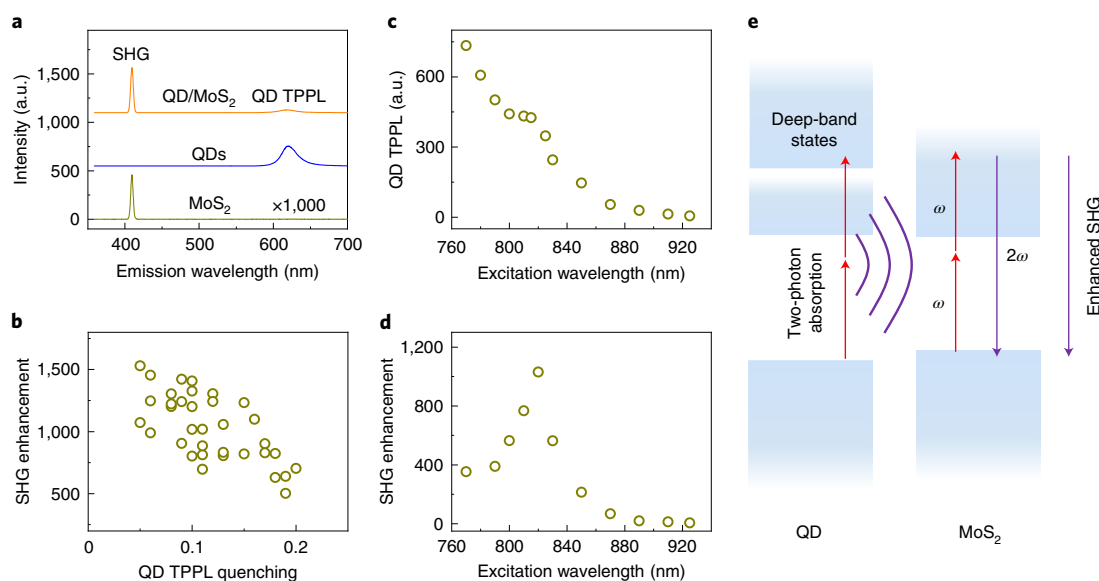


Fig. 3 | Excitation-wavelength-dependent SHG enhancement. **a**, SHG and TPPL spectra of the pristine MoS₂ monolayer, QD film and their hybrid under 820 nm pulsed-laser excitation. The sharp peak at 410 nm is the SHG of MoS₂ and the broader peak at 620 nm corresponds to the TPPL of the QDs. Compared with its component layers, the QD/MoS₂ hybrid shows an enhanced MoS₂ SHG and a quenched QD TPPL. **b**, The MoS₂ SHG enhancement versus QD TPPL quenching in the hybrid structure obtained from around 40 samples. When the SHG was enhanced more noticeably, the QD TPPL was quenched more significantly. **c,d**, Wavelength-dependent TPPL of the pristine QD film (**c**) and SHG enhancement in the QD/MoS₂ hybrid (**d**) under two-photon excitation. The TPPL spectrum of the QDs presents a shoulder around ~ 820 nm, indicating the existence of deep-band excited states with a strong oscillator strength and high two-photon absorption. By coincidence, the SHG enhancement in the hybrid shows a peak at ~ 820 nm as well. **e**, Scheme of multiphoton-excitation resonance energy transfer and SHG enhancement. Under resonant excitation of the deep-band two-photon excited states in the QDs, strong dipole coupling and perfect energy overlap between the QDs and MoS₂ facilitate the high-efficiency energy transfer and hence substantially strengthen the second harmonic response.

To gain a deeper insight into the mechanism, we applied wavelength-dependent two-photon excitation measurements. Figure 3a shows the reflective spectra containing the SHG and the TPPL of the MoS₂ monolayer, the QD film and their hybrid under 820 nm pulsed-laser excitation. These spectra feature sharp peaks at 410 nm and broader peaks at 620 nm, corresponding to the SHG signal from MoS₂ and the TPPL signal from the QDs, respectively. As expected, the large two-photon absorption cross-section and the high PL quantum efficiency give the QDs a high TPPL conversion efficiency of up to $\sim 2 \times 10^{-3}$ (fundamental pump peak intensity of 20 GW cm^{-2}). Here we note that no detectable TPPL from pristine MoS₂ can be observed under the same conditions. After QD coating,

the SHG of MoS₂ in the hybrid is enhanced by three orders of magnitude. Meanwhile, the TPPL of the QDs in the hybrid is quenched to around one-tenth of the pristine QD film. To understand the relationship between SHG enhancement and TPPL quenching (defined as the TPPL intensity in QD/MoS₂ compared with that in the pristine QDs), we tested approximately 40 hybrid samples and found that the stronger SHG in MoS₂ is always accompanied by weaker TPPL in the QDs (Fig. 3b). This observation is also consistent with the interaction-distance-dependent TPPL of the QDs in the QD/SiO₂/MoS₂ hybrid system, where the insertion of the SiO₂ spacer layer weakens the SHG enhancement and increases the TPPL intensity at the same time (Supplementary Fig. 5).

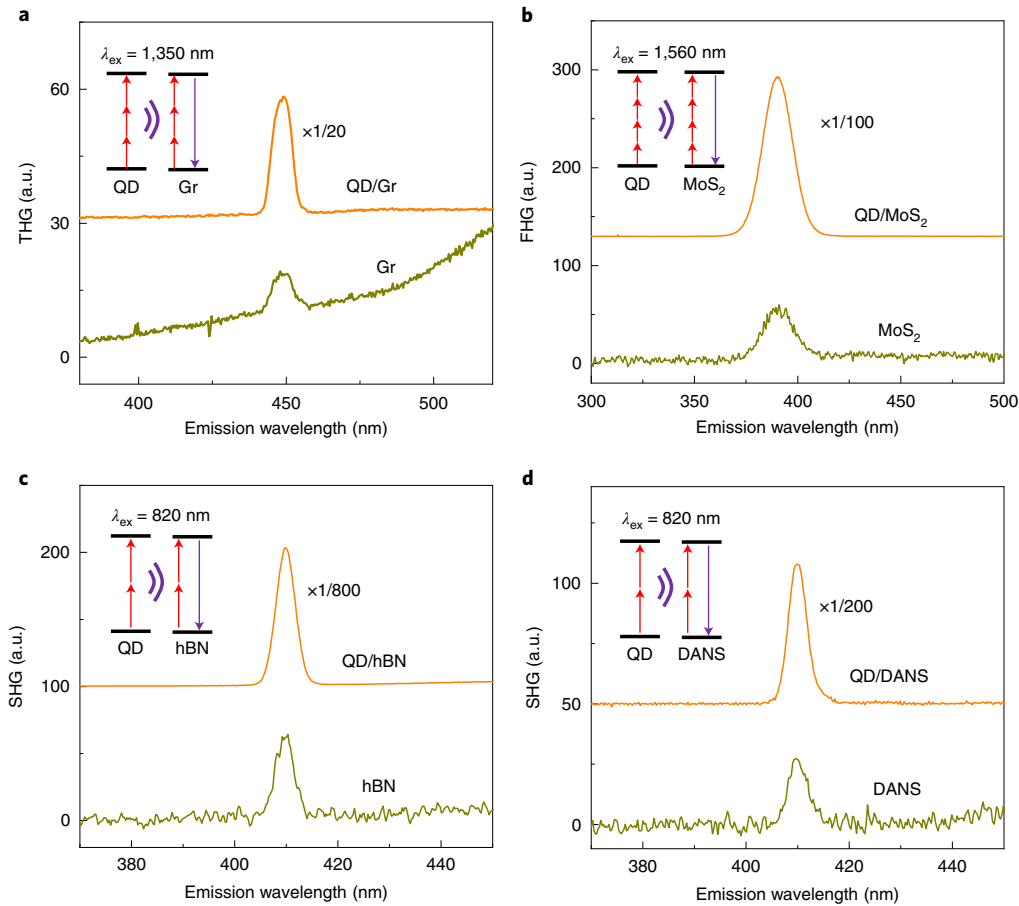


Fig. 4 | Universal optical nonlinearity enhancement of various 2D systems with different frequency harmonic orders. **a, b**, Enhancement of high-order frequency harmonic generations. After QD coating, both the THG of conducting graphene under excitation at 1,350 nm (**a**) and the FHG of semiconducting MoS₂ under excitation at 1,560 nm (**b**) are enhanced. Gr, graphene. **c, d**, Optical nonlinearity enhancement of various 2D systems. Beside conducting graphene and semiconducting MoS₂, QD coating can also enhance the SHG of insulating hBN (**c**) and DANS (**d**) thin molecular films. The excitation wavelength for SHG is 820 nm. The insets schematically illustrate the multiphoton-excitation resonance energy transfer from the QDs to the 2D materials for optical nonlinearity enhancement.

In the wavelength-dependent two-photon excitation experiments with excitation wavelength tuned from 925 to 770 nm, the TPPL intensity of the QDs shows a continuous increase and a shoulder is seen at around 820 nm (Fig. 3c). This shoulder is attributed to deep-band states obeying the selection rule of two-photon absorption and hints at the strong oscillator strength. By coincidence, the SHG enhancement in the hybrid also shows a peak at ~820 nm (Fig. 3d). Further controlled experiments using the QD/WS₂ hybrid show that the SHG enhancement of WS₂ presents a peak at ~820 nm as well (Supplementary Fig. 6), although the shape of the wavelength-dependent SHG spectrum of WS₂ is different from that of MoS₂. Therefore, the peak in Fig. 3d must stem from the properties of the QDs rather than from the 2D materials. We can safely conclude that the enhancement of the SHG in MoS₂ is directly correlated to the strong two-photon absorption and the associated TPPL quenching in the QDs.

Based on all of the above experiments, here we propose a mechanism for multiphoton-excitation resonance energy transfer to understand the greatly enhanced SHG in MoS₂ by the QD coating, where the second harmonic response dipole in MoS₂ directly gains energy from the two-photon absorption dipole with a strong oscillator strength in the QDs by a high-efficiency remote Coulombic coupling (Fig. 3e)³⁰. Generally, the energy-transfer rate k^{ET} is determined by two terms, the energy

overlap $\int_0^\infty d\varepsilon J(\varepsilon)$ and the Coulombic coupling strength $V_{\text{coupling}}^{\text{Coul}}$, which can be described as

$$k^{\text{ET}} = \frac{2\pi}{\hbar} \left| V_{\text{coupling}}^{\text{Coul}} \right|^2 \int_0^\infty d\varepsilon J(\varepsilon), \quad (1)$$

$$V_{\text{coupling}}^{\text{Coul}} = \frac{e^2}{4\pi\epsilon_0} \int \frac{P^{\text{D}}(\mathbf{r}_1) P^{\text{A}}(\mathbf{r}_2)}{|\mathbf{r}_1 - \mathbf{r}_2|} d\mathbf{r}_1 d\mathbf{r}_2. \quad (2)$$

Here, the energy overlap is expressed as an overlap between the donor emission spectrum $f^{\text{D}}(\varepsilon)$ and the acceptor absorption spectrum $f^{\text{A}}(\varepsilon)$, each of which has been normalized to the unit area on energy scale, as $J(\varepsilon) = f^{\text{D}}(\varepsilon) f^{\text{A}}(\varepsilon)$. The Coulombic coupling strength $V_{\text{coupling}}^{\text{Coul}}$ is determined by quantum mechanical oscillator transition densities of the donor polarization $P^{\text{D}}(\mathbf{r}_1)$ and acceptor polarization $P^{\text{A}}(\mathbf{r}_2)$. Therefore, adapting the donor and acceptor materials for a large energy overlap and engineering the coupling strength are two main strategies for obtaining efficient energy transfer.

For traditional linear-excitation energy transfer, such as in fluorescence resonance energy transfer, the donor emission spectrum only overlaps with the side bands of the acceptor absorption spectrum, resulting in relatively small values of energy overlap $J(\varepsilon)$. But here for the multiphoton-excitation resonance energy trans-

fer, the two-photon absorption spectrum in the QDs and the SHG of MoS₂ have nearly perfect overlap, guaranteeing the near-unity $\int_0^\infty d\epsilon J(\epsilon)$ (Supplementary Fig. 7). Meanwhile, the QDs are an ideal photoexcited-energy-storage material with generally strong two-photon absorption. Especially under resonant excitation of those deep-band states¹⁰, the strong dipole oscillator strength in the QDs gives massive stored energy and strong Coulombic coupling with the adjacent MoS₂. These two unique factors of the QDs together contribute to the high-efficiency energy transfer

$$(\eta = 1 - \frac{\text{TPPL}_{2\text{D-QD}}}{\text{TPPL}_{\text{QD}}} = 95\% \text{ under QD TPPL quenching of } \sim 0.05)$$

and hence can strengthen the second harmonic response of MoS₂ by up to $\sim 1,500$ times. Under this model, the effective coupling radius R_0 , where the energy-transfer efficiency drops to 50%, is given as ~ 17 nm. It is worth noting that the energy-transfer rate should scale as R^{-4} for a perfect 0D–2D dipole–dipole interaction system from previous calculations³⁵. However, in our experiments, the QDs have a finite size of ~ 10 nm and form a film structure (\sim sub-200 nm thickness). This might explain why our data show the salient feature of $R^{-2.3}$ -dependent energy transfer³⁹.

Under multiphoton resonant excitation of the deep-band states with the strong oscillator strength in the QDs, our enhancement mechanism is expected to be quite universal for different nonlinear harmonic orders and various 2D forms, as the nonlinear high-order absorption in the QDs and the same order harmonic generation in the 2D materials are always of the same wavelength and have nearly perfect spectral overlap. For example, under 1,350 nm excitation, the resonant three-photon absorption in the QDs and third harmonic generation (THG) in graphene both happen at 450 nm, resulting in the strong THG enhancement in conducting graphene after QD coating (Fig. 4a), via a three-photon-excitation energy-transfer process (inset of Fig. 4a). Moreover, the high enhancement is observed in the fourth harmonic generation (FHG) at 390 nm in QD/MoS₂ under excitation at 1,560 nm (Fig. 4b). In addition, by coating QDs on insulating hBN (Fig. 4c) or organic DANS (Fig. 4d) thin molecular films, the SHG signal can also be enhanced, indicating that QD coating is a universal method for enhancing the nonlinear optical responses of different 2D materials. We notice that the absolute enhancement factor varies in different nonlinear orders and 2D systems, and currently we do not have a quantitative understanding of this difference. In the near future, more theoretical exploration of the excited dynamics should be carried out and may provide more in-depth information on the multiphoton-excitation resonance energy transfer⁴⁰.

In summary, we demonstrated a universal route for spatially homogeneous and giant enhancement of the nonlinear optical responses of 2D systems by high-efficiency remote multiphoton-excitation resonance energy transfer from adjacent QDs. The greatly enhanced nonlinear light–matter interactions in 2D materials, together with their facile compatibility with current microfabrication technology, should open up exciting opportunities in the design of optoelectronic and nanophotonic devices.

Online content

Any methods, additional references, Nature Research reporting summaries, source data, extended data, supplementary information, acknowledgements, peer review information; details of author contributions and competing interests; and statements of data and code availability are available at <https://doi.org/10.1038/s41566-021-00801-2>.

Received: 12 June 2020; Accepted: 19 March 2021;

Published online: 29 April 2021

References

1. Kamat, P. V. Quantum dot solar cells. Semiconductor nanocrystals as light harvesters. *J. Phys. Chem. C* **112**, 18737–18753 (2008).

2. Kim, T.-H. et al. Full-colour quantum dot displays fabricated by transfer printing. *Nat. Photonics* **5**, 176–182 (2011).
3. Qian, L., Zheng, Y., Xue, J. & Holloway, P. H. Stable and efficient quantum-dot light-emitting diodes based on solution-processed multilayer structures. *Nat. Photonics* **5**, 543–548 (2011).
4. Konstantatos, G. et al. Hybrid graphene–quantum dot phototransistors with ultrahigh gain. *Nat. Nanotechnol.* **7**, 363–368 (2012).
5. Shirasaki, Y., Supran, G. J., Bawendi, M. G. & Bulović, V. Emergence of colloidal quantum-dot light-emitting technologies. *Nat. Photonics* **7**, 13–23 (2013).
6. Bao, J. & Bawendi, M. G. A colloidal quantum dot spectrometer. *Nature* **523**, 67–70 (2015).
7. Adinolfi, V. & Sargent, E. H. Photovoltage field-effect transistors. *Nature* **542**, 324–327 (2017).
8. Tang, X., Ackerman, M. M., Chen, M. & Guyot-Sionnest, P. Dual-band infrared imaging using stacked colloidal quantum dot photodiodes. *Nat. Photonics* **13**, 277–282 (2019).
9. Hanifi, D. A. et al. Redefining near-unity luminescence in quantum dots with photothermal threshold quantum yield. *Science* **363**, 1199–1202 (2019).
10. Allione, M. et al. Two-photon-induced blue shift of core and shell optical transitions in colloidal CdSe/CdS quasi-type II quantum rods. *ACS Nano* **7**, 2443–2452 (2013).
11. Wang, Y. et al. Stimulated emission and lasing from CdSe/CdS/ZnS core–multi-shell quantum dots by simultaneous three-photon absorption. *Adv. Mater.* **26**, 2954–2961 (2014).
12. Makarov, N. S. et al. Two-photon absorption in CdSe colloidal quantum dots compared to organic molecules. *ACS Nano* **8**, 12572–12586 (2014).
13. Wang, Y. et al. Structural phase transition in monolayer MoTe₂ driven by electrostatic doping. *Nature* **550**, 487–491 (2017).
14. Liu, H. et al. High-harmonic generation from an atomically thin semiconductor. *Nat. Phys.* **13**, 262–265 (2017).
15. Yoshikawa, N., Tamaya, T. & Tanaka, K. High-harmonic generation in graphene enhanced by elliptically polarized light excitation. *Science* **356**, 736–738 (2017).
16. Sie, E. J. et al. An ultrafast symmetry switch in a Weyl semimetal. *Nature* **565**, 61–66 (2019).
17. Wu, S. et al. Monolayer semiconductor nanocavity lasers with ultralow thresholds. *Nature* **520**, 69–72 (2015).
18. Sun, Z., Martinez, A. & Wang, F. Optical modulators with 2D layered materials. *Nat. Photonics* **10**, 227–238 (2016).
19. Yao, B. et al. Gate-tunable frequency combs in graphene–nitride microresonators. *Nature* **558**, 410–414 (2018).
20. Li, Y. et al. Probing symmetry properties of few-layer MoS₂ and h-BN by optical second-harmonic generation. *Nano Lett.* **13**, 3329–3333 (2013).
21. Cheng, J.-L., Vermeulen, N. & Sipe, J. Third order optical nonlinearity of graphene. *New J. Phys.* **16**, 053014 (2014).
22. Seyler, K. L. et al. Electrical control of second-harmonic generation in a WSe₂ monolayer transistor. *Nat. Nanotechnol.* **10**, 407–411 (2015).
23. Liang, J. et al. Monitoring local strain vector in atomic-layered MoSe₂ by second-harmonic generation. *Nano Lett.* **17**, 7539–7543 (2017).
24. Jiang, T. et al. Gate-tunable third-order nonlinear optical response of massless Dirac fermions in graphene. *Nat. Photonics* **12**, 430–436 (2018).
25. Soavi, G. et al. Broadband, electrically tunable third-harmonic generation in graphene. *Nat. Nanotechnol.* **13**, 583–588 (2018).
26. Aouani, H., Rahmani, M., Navarro-Cia, M. & Maier, S. A. Third-harmonic-upconversion enhancement from a single semiconductor nanoparticle coupled to a plasmonic antenna. *Nat. Nanotechnol.* **9**, 290–294 (2014).
27. Lee, J. et al. Giant nonlinear response from plasmonic metasurfaces coupled to intersubband transitions. *Nature* **511**, 65–69 (2014).
28. Wen, X., Xu, W., Zhao, W., Khurgin, J. B. & Xiong, Q. Plasmonic hot carriers-controlled second harmonic generation in WSe₂ bilayers. *Nano Lett.* **18**, 1686–1692 (2018).
29. Shi, J. et al. Efficient second harmonic generation in a hybrid plasmonic waveguide by mode interactions. *Nano Lett.* **19**, 3838–3845 (2019).
30. Scholes, G. D. Long-range resonance energy transfer in molecular systems. *Annu. Rev. Phys. Chem.* **54**, 57–87 (2003).
31. Hernández-Martínez, P. L., Govorov, A. O. & Demir, H. V. Generalized theory of Förster-type nonradiative energy transfer in nanostructures with mixed dimensionality. *J. Phys. Chem. C* **117**, 10203–10212 (2013).
32. Cox, J. D. & Garcia de Abajo, F. J. Nonlinear atom-plasmon interactions enabled by nanostructured graphene. *Phys. Rev. Lett.* **121**, 257403 (2018).
33. Achermann, M. et al. Energy-transfer pumping of semiconductor nanocrystals using an epitaxial quantum well. *Nature* **429**, 642–646 (2004).
34. Tisdale, W. A. et al. Hot-electron transfer from semiconductor nanocrystals. *Science* **328**, 1543–1547 (2010).

35. Gaudreau, L. et al. Universal distance-scaling of nonradiative energy transfer to graphene. *Nano Lett.* **13**, 2030–2035 (2013).
36. Rowland, C. E. et al. Picosecond energy transfer and multiexciton transfer outpaces Auger recombination in binary CdSe nanoplatelet solids. *Nat. Mater.* **14**, 484–489 (2015).
37. Raja, A. et al. Energy transfer from quantum dots to graphene and MoS₂: the role of absorption and screening in two-dimensional materials. *Nano Lett.* **16**, 2328–2333 (2016).
38. Zhu, X. et al. Charge transfer excitons at van der Waals interfaces. *J. Am. Chem. Soc.* **137**, 8313–8320 (2015).
39. Prins, F., Goodman, A. J. & Tisdale, W. A. Reduced dielectric screening and enhanced energy transfer in single- and few-layer MoS₂. *Nano Lett.* **14**, 6087–6091 (2014).
40. Engelmann, A., Yudson, V. & Reineker, P. Enhanced optical nonlinearity of hybrid excitons in an inorganic semiconducting quantum dot covered by an organic layer. *Phys. Rev. B* **57**, 1784–1790 (1998).

Publisher's note Springer Nature remains neutral with regard to jurisdictional claims in published maps and institutional affiliations.

© The Author(s), under exclusive licence to Springer Nature Limited 2021

Methods

Synthesis of CdSe/ZnS core/shell colloidal quantum dots. A mixture of selenium (0.158 g, 2 mmol), octadecylamine (1.62 g, 6 mmol) and 1-octadecene (90% 20 ml) was heated to 120 °C for 30 min, and then to 220 °C for 4 h to prepare the selenium precursor. A mixture of ZnO (0.326 g, 4 mmol), oleic acid (5.64 g, 16 mmol) and 1-octadecene (13.7 ml) was heated to 310 °C to prepare the zinc solution precursor. CdO (0.0154 g, 0.12 mmol), stearic acid (0.36 mmol) and 1-octadecene were mixed and heated to 280 °C under nitrogen flow. Then the prepared selenium precursor (2 ml) was injected. When the colour had turned dark red, the mixture was cooled to room temperature and the CdSe nanocrystals were prepared. The as-prepared CdSe nanocrystals were first purified by repeated precipitation with methanol several times and then dispersed in hexanes. 1-Octadecene (3 ml), octadecylamine (1 g) and the purified CdSe core in hexanes were mixed at 100 °C under nitrogen flow for 20 min to remove the hexanes. Subsequently, the solution was heated to ~180–280 °C for growth of the shells. The linear absorption and PL spectra of the CdSe/ZnS QDs with a band gap of 620 nm used in our experiments are shown in Supplementary Fig. 8.

Fabrication of quantum dot hybrid. A triangular-shaped MoS₂ monolayer was grown on a SiO₂/Si substrate via a chemical vapour deposition process using MoO₃ and sulfur powder as the precursors at atmospheric pressure. Then a hBN monolayer was grown on copper foil and transferred to the SiO₂/Si substrate. A graphene monolayer was exfoliated on fused silica. The DANS molecule was spin coated on the SiO₂/Si substrate. Then the CdSe/ZnS core/shell QD film was deposited on MoS₂, hBN, graphene or DANS by spin coating. The thickness of the QD film on each 2D material can be controlled by the QD solution concentration and the spin-coating conditions. For different 2D materials, the QD coating thicknesses can be different.

Harmonic generation measurements. Two systems were alternatively used in our harmonic generation measurement. Wavelength-dependent SHG was excited using a Spectra-Physics Mai Tai oscillator (~100 fs, 80 MHz, 690–1,050 nm). THG and FHG were excited using a Coherent Vitara-T oscillator and an optical parametric amplifier 9850 laser system (~70 fs, 250 kHz, 1,200–1,600 nm). The excitation laser was focused using a Nikon objective (×60, NA = 0.65) and the harmonic generation signal was collected by the same objective in reflection mode. After filtering out the excitation laser, the harmonic generation signal was recorded using a Princeton SP2500 spectrometer equipped with a nitrogen-cooled silicon charge coupled device camera. For the polarization-dependent SHG pattern, we recorded the SHG with polarization parallel to that of the excitation laser. The experimental

scheme is shown in our previous work²³. All our experiments were carried out at room temperature.

Acknowledgements

This work was supported by the National Natural Science Foundation of China (52025023, 51991342, 52021006, 51722204, 51972041, 51972042, 51672007, 11974023, 12025407 and 11934003), the National Key R&D Program of China (2016YFA0300903 and 2016YFA0300804), Beijing Natural Science Foundation (JQ19004), Beijing Excellent Talents Training Support (2017000026833ZK11), the Strategic Priority Research Program of the Chinese Academy of Sciences (XDB33000000), Beijing Municipal Science & Technology Commission (Z191100007219005), Beijing Graphene Innovation Program (Z181100004818003), Key-Area Research and Development Program of Guangdong Province (2020B010189001, 2019B010931001 and 2018B030327001), the Science, Technology and Innovation Commission of Shenzhen Municipality (KYTDPT20181011104202253), Bureau of Industry and Information Technology of Shenzhen (Graphene platform 201901161512), The Pearl River Talent Recruitment Program of Guangdong Province (2019ZT08C321), National Equipment Program of China (ZDYZ2015-1) and the China Postdoctoral Science Foundation (2020M680177).

Author contributions

Kaihui Liu designed the experiments. Kaihui Liu and J.X. supervised the project. H.H., C.W. and Z.Z. performed the frequency harmonic generation experiments. F.W., J.F., H.S. and Y.W. prepared the QD samples. Y.Zuo, J.W., C.L. and Y.Zhao grew MoS₂ and WS₂ samples. J.Z., J.Y., Kehai Liu, P.G., S.M., S.W. and Z.S. suggested the optical experiments. Kaihui Liu and H.H. wrote the manuscript. All authors contributed to the scientific discussion and modifying the manuscript.

Competing interests

The authors declare no competing interests.

Additional information

Supplementary information The online version contains supplementary material available at <https://doi.org/10.1038/s41566-021-00801-2>.

Correspondence and requests for materials should be addressed to K.L. or J.X.

Peer review information *Nature Photonics* thanks the anonymous reviewers for their contribution to the peer review of this work.

Reprints and permissions information is available at www.nature.com/reprints.